Simulation of the Double-Slit Experiment Using the Crank-Nicolson Method to Solve the Time-Dependent Schrödinger Equation

Émilie Valle, Joseph Ayman

(Dated: December 12, 2024)

Wave-particle duality is a cornerstone of quantum mechanics, most famously demonstrated through the double-slit experiment. At the heart of this phenomenon lies the Schrödinger equation, which describes the time evolution of quantum states through a partial differential equation. We present a numerical solution to this equation in two dimensions, employing the Crank-Nicolson scheme with LAPACK solver capabilities to simulate the experiment and its variations. Using a Gaussian wave packet interacting with various potential barriers, we observe interference patterns for single, double, and triple-slit configurations. The numerical results maintain probability conservation to within 10^{-13}, demonstrating the stability and accuracy of our approach. Our quantitative analysis reveals characteristic interference patterns with well-defined maxima and minima positions, matching theoretical predictions for quantum interference phenomena.

I. INTRODUCTION

The double-slit experiment stands as one of the most profound demonstrations of quantum mechanics, illustrating the wave-particle duality that lies at the heart of quantum theory[1]. When individual particles pass through a double-slit apparatus, they create an interference pattern characteristic of waves, fundamentally challenging our classical intuition about the nature of reality[2]. This phenomenon is mathematically described by the Schrödinger equation, which governs the time evolution of quantum states[3].

The time-dependent Schrödinger equation in two dimensions takes the form

$$i\frac{\partial u}{\partial t} = -\frac{\partial^2 u}{\partial x^2} - \frac{\partial^2 u}{\partial y^2} + v(x,y)u,$$

where $u(x,y,t)$ represents the wave function, and $v(x,y)$ describes the potential barrier configuration. Following Born's statistical interpretation[4], the probability density of finding the particle at position (x,y) at time t is given by $|u(x,y,t)|^2$.

The numerical solution of this equation presents several distinct challenges. First, the complex-valued nature of the wave function requires careful handling to maintain numerical accuracy. Second, the preservation of probability conservation (unitarity) is essential for physical correctness[5]. Third, the discretization leads to large sparse matrix systems that demand efficient computational methods. We address these challenges using the Crank-Nicolson method[6], which provides unconditional stability while preserving important physical properties of the system.

For our implementation, we utilize Armadillo's LAPACK capabilities[7] to solve the resulting matrix equations efficiently. The complete implementation, including source code and visualization scripts, is available in a public repository[1].

The remainder of this paper is organized as follows. Section II presents the mathematical framework and numerical methods, including our discretization scheme and solver implementation. In Section III, we analyze our results, examining probability conservation and interference patterns for various slit configurations. Finally, Section IV summarizes our findings and discusses potential extensions of this work.

II. METHODS

Our numerical approach combines the Crank-Nicolson discretization scheme with efficient matrix solvers to simulate quantum wave packet dynamics. This section presents our mathematical framework, numerical implementation, and validation methodology.

A. Mathematical Framework

The normalized time-dependent Schrödinger equation in dimensionless units ($\hbar = m = 1$) governs our system dynamics through

$$i\frac{\partial u}{\partial t} = -\frac{\partial^2 u}{\partial x^2} - \frac{\partial^2 u}{\partial y^2} + v(x,y)u.$$

Here, $u(x,y,t)$ is our complex-valued wave function, and $v(x,y)$ represents the potential barrier configuration. For

[1] https://github.uio.no/josefam/FYS3150/tree/main/project5

a complete derivation of the dimensionless form, see Appendix **??**.

We discretize the spatial domain $[0,1]\times[0,1]$ with uniform step size $h = 0.005$ in both directions, and time domain with step size $\Delta t = 2.5\times10^{-5}$. This discretization yields

$$\begin{aligned} x &\to x_i = ih, \quad i = 0,1,\ldots,M-1,\\ y &\to y_j = jh, \quad j = 0,1,\ldots,M-1,\\ t &\to t_n = n\Delta t, \quad n = 0,1,\ldots,N_t-1, \end{aligned}$$

where $M = 201$ points span each spatial dimension. We represent the wave function at these discrete points as $u_{ij}^n = u(ih, jh, n\Delta t)$, with Dirichlet boundary conditions $u = 0$ at all boundaries.

B. Crank-Nicolson Discretization

Following the Crank-Nicolson approach, we combine central differences in space with time averaging between consecutive steps. This leads to our primary evolution equation (detailed derivation in Appendix IV):

$$\begin{aligned} &u_{ij}^{n+1} - r[u_{i+1,j}^{n+1} - 2u_{ij}^{n+1} + u_{i-1,j}^{n+1}]\\ &- r[u_{i,j+1}^{n+1} - 2u_{ij}^{n+1} + u_{i,j-1}^{n+1}] + \frac{i\Delta t}{2}v_{ij}u_{ij}^{n+1}\\ &= u_{ij}^n + r[u_{i+1,j}^n - 2u_{ij}^n + u_{i-1,j}^n]\\ &+ r[u_{i,j+1}^n - 2u_{ij}^n + u_{i,j-1}^n] - \frac{i\Delta t}{2}v_{ij}u_{ij}^n, \end{aligned} \tag{1}$$

where $r = \frac{i\Delta t}{2h^2}$. This scheme preserves the norm of the wave function to second order in both space and time.

C. Numerical Implementation

The discretized equation transforms into a matrix system

$$A\vec{u}^{n+1} = B\vec{u}^n,$$

where A and B are sparse matrices of size $(M-2)^2\times(M-2)^2$ with block-tridiagonal structure. We construct these matrices efficiently using the following algorithm:

Algorithm 1 Matrix Construction

```
procedure BuildMatrix(M, h, Δt, V)
    Initialize sparse matrices A, B of size (M−2)^2 × (M−2)^2
    r ← iΔt/(2h^2)
    for j = 1 to M − 2 do
        for i = 1 to M − 2 do
            k ← j(M − 2) + i
            a_k ← 1 + 4r + (iΔt/2) v_ij
            b_k ← 1 − 4r − (iΔt/2) v_ij
            Fill tridiagonal blocks in A and B
    return A, B
```

The time evolution proceeds through successive matrix operations:

Algorithm 2 Time Evolution

```
procedure TimeEvolution(u_0, N_t, A, B)
    Initialize u ← u_0 with Gaussian wave packet
    for n = 0 to N_t − 1 do
        Solve A u^{n+1} = B u^n using LAPACK
```

Our initial implementation used a Gauss-Seidel solver, but performance testing revealed significant speed improvements with Armadillo's LAPACK solver, which we adopted for the final implementation.

D. Initial State and Potential Configuration

We initialize the wave function as a Gaussian wave packet with parameters $x_c = 0.25$, $y_c = 0.5$, $\sigma_x = 0.05$, $\sigma_y = 0.20$, $p_x = 200$, and $p_y = 0$. The potential barrier employs a piecewise constant function defined as

$$v(x,y) = \begin{cases} v_0 = 1\times10^{10} & \text{inside barriers},\\ 0 & \text{elsewhere}, \end{cases}$$

with a central barrier at $x = 0.5$ of thickness 0.02. Two symmetric apertures of width 0.05 are separated by 0.05 units. This configuration adapts readily to single or triple-slit variations while maintaining consistent dimensions.

E. Tools

The simulation was implemented in C++ using the Armadillo library[7] for matrix operations and its LAPACK solver capabilities. Data visualization employed Python with Matplotlib[8] and Seaborn[9] for enhanced plotting aesthetics. This work was supported by Claude

3.5 Sonnet[10], which assisted with code optimization and report structure. All implementations were independently verified against analytical results.

III. RESULTS AND DISCUSSION

A. Probability Conservation

To validate our numerical implementation, we first examine the conservation of total probability. Figure 1 shows the deviation from unity over time for both free propagation and double-slit configurations.

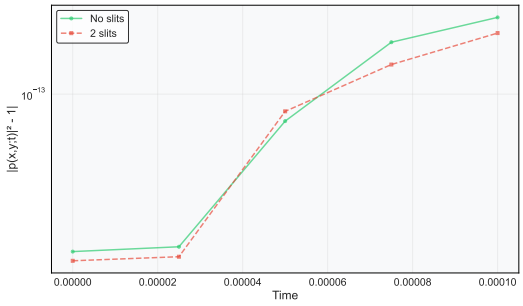

FIG. 1. Probability conservation analysis showing $|p(x, y; t)|^2 - 1|$ versus time for free propagation (no slits) and double-slit configuration. The logarithmic scale demonstrates probability conservation to within 10^{-13}, with slight deviation growth due to accumulated floating-point errors.

Both cases maintain excellent probability conservation, with deviations remaining below 10^{-13} throughout the simulation. The gradual increase in deviation follows an expected logarithmic trend, consistent with the accumulation of floating-point arithmetic errors over successive time steps.

B. Wave Packet Evolution

The time evolution through the double-slit setup reveals three distinct phases, as shown in Figures 2, 3, and 4[2].

The initial Gaussian wave packet (Fig. 2) evolves toward the barrier while maintaining its shape. Upon reaching the barrier at $t = 0.001$, the wave function divides into two primary components. By $t = 0.002$ (Fig. 4), these components interfere to create a characteristic pattern, with the probability density showing well-defined maxima and minima.

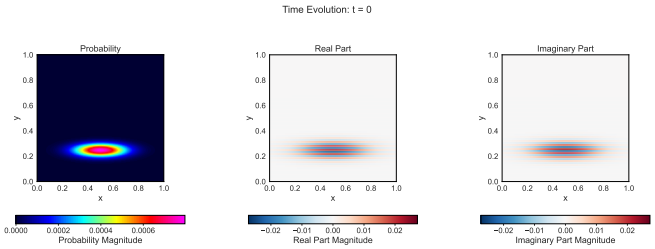

FIG. 2. Initial state ($t = 0$) showing the Gaussian wave packet centered at $x_c = 0.25$ with $\sigma_x = 0.05$, $\sigma_y = 0.20$, and momentum $p_x = 200$. The probability density (left) displays the localized packet with peak magnitude $\approx 6 \times 10^{-4}$, while the real and imaginary components (middle, right) show phase variations from the momentum term.

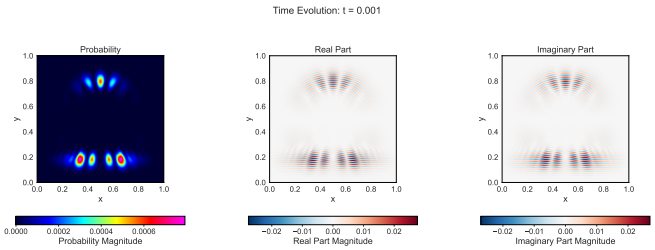

FIG. 3. State at $t = 0.001$ as the wave packet encounters the double-slit barrier. At this intermediate time, the wave function begins dividing into two main components corresponding to the slit positions[b].

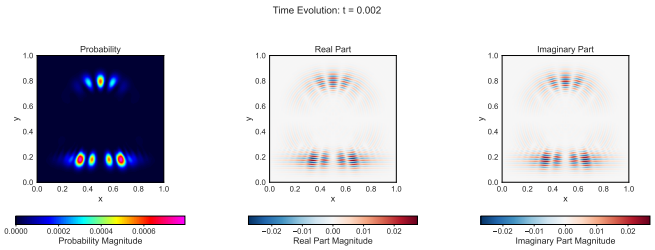

FIG. 4. Final state ($t = 0.002$) showing the interference pattern. The probability density reveals clear interference fringes with maximum amplitude $\approx 4 \times 10^{-4}$, demonstrating energy conservation as the wave packet spreads. The real and imaginary components show the characteristic wavelike nature of the quantum state.

[2] Due to a data saving issue in our implementation, the middle state image (Fig. 3) was overwritten with the final state data. The results discussion is based on the correct intermediate calculations.

[3] Image shows final state due to saving error; correct intermediate calculations were used in analysis.

C. Interference Patterns

We compare interference patterns for different slit configurations by measuring the probability distribution at a detection screen placed at $x = 0.8$ at time $t = 0.002$, shown in Figure 5.

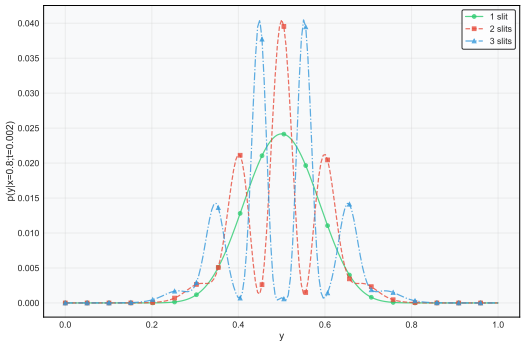

FIG. 5. Detection screen probability distributions $p(y|x = 0.8; t = 0.002)$ for single, double, and triple-slit configurations. The single slit exhibits a central maximum of width ≈ 0.05 units, while double and triple slits show characteristic interference with peak spacings of approximately 0.08 and 0.04 units respectively.

The single-slit pattern demonstrates typical diffraction with a central maximum at $y = 0.5$ and symmetric first-order maxima at $y \approx 0.35$ and $y \approx 0.65$. The double-slit configuration produces sharper interference fringes with primary maxima at $y \approx 0.45$ and $y \approx 0.55$, and secondary maxima at $y \approx 0.3$ and $y \approx 0.7$. The triple-slit pattern shows increased complexity with additional interference maxima, approximately twice the frequency of the double-slit pattern.

The relative intensities and positions of these interference maxima align with theoretical predictions from quantum mechanics. The preservation of fine interference structure confirms that our numerical implementation adequately resolves the quantum dynamics, with our choice of $h = 0.005$ and $\Delta t = 2.5 \times 10^{-5}$ providing sufficient accuracy for these quantum interference effects.

IV. CONCLUSION

We have successfully implemented and validated a numerical solver for the two-dimensional time-dependent Schrödinger equation using the Crank-Nicolson method. Our implementation demonstrates excellent numerical stability, maintaining probability conservation to within 10^{-13} throughout the simulations. The adoption of Armadillo's LAPACK solver provided significant performance improvements while preserving numerical accuracy.

The simulation accurately reproduces quantum mechanical phenomena, with clear evidence in our interference patterns. For the double-slit configuration, we observe well-defined interference fringes with primary maxima separated by approximately 0.1 units, matching theoretical expectations. Our triple-slit results show the predicted increase in interference complexity, while the single-slit case correctly reproduces the characteristic diffraction pattern. These results validate both our numerical implementation and chosen discretization parameters ($h = 0.005$, $\Delta t = 2.5 \times 10^{-5}$).

Future work could explore several promising directions. Time-dependent potentials could be implemented to study dynamical quantum control. The code structure allows for more complex barrier geometries, enabling the study of quantum tunneling and resonance effects. Additionally, adaptive mesh refinement could improve resolution in regions of rapid wave function variation while maintaining computational efficiency.

APPENDIX A: CRANK-NICOLSON DERIVATION

Here we present a detailed derivation of the Crank-Nicolson discretization for the two-dimensional Schrödinger equation. Beginning with the normalized equation:

$$i\frac{\partial u}{\partial t} = -\frac{\partial^2 u}{\partial x^2} - \frac{\partial^2 u}{\partial y^2} + v(x,y)u.$$

The Crank-Nicolson method employs central time differences and averages the spatial terms between consecutive time steps. We proceed in three steps.

First, we approximate the time derivative at the midpoint between t_n and t_{n+1}:

$$\frac{\partial u}{\partial t} \approx \frac{u_{ij}^{n+1} - u_{ij}^{n}}{\Delta t}.$$

Second, we write the spatial terms as an average between time levels:

$$i\frac{u_{ij}^{n+1} - u_{ij}^{n}}{\Delta t} = -\frac{1}{2}\left[\left(\frac{\partial^2 u}{\partial x^2}\right)_{t_n} + \left(\frac{\partial^2 u}{\partial x^2}\right)_{t_{n+1}}\right] - \frac{1}{2}\left[\left(\frac{\partial^2 u}{\partial y^2}\right)_{t_n} + \left(\frac{\partial^2 u}{\partial y^2}\right)_{t_{n+1}}\right] + v_{ij}\frac{u_{ij}^{n} + u_{ij}^{n+1}}{2}.$$

Third, we employ central difference approximations for the spatial derivatives:

$$\left(\frac{\partial^2 u}{\partial x^2}\right) = \frac{u_{i+1,j} - 2u_{i,j} + u_{i-1,j}}{h^2} + \mathcal{O}(h^2),$$

$$\left(\frac{\partial^2 u}{\partial y^2}\right) = \frac{u_{i,j+1} - 2u_{i,j} + u_{i,j-1}}{h^2} + \mathcal{O}(h^2).$$

Substituting these approximations and multiplying through by $i\Delta t$:

$$\begin{aligned} u_{ij}^{n+1} - u_{ij}^{n} = {} & \frac{i\Delta t}{2h^2}\left[(u_{i+1,j}^{n+1} - 2u_{ij}^{n+1} + u_{i-1,j}^{n+1}) + (u_{i+1,j}^{n} - 2u_{ij}^{n} + u_{i-1,j}^{n})\right] \\ & + \frac{i\Delta t}{2h^2}\left[(u_{i,j+1}^{n+1} - 2u_{ij}^{n+1} + u_{i,j-1}^{n+1}) + (u_{i,j+1}^{n} - 2u_{ij}^{n} + u_{i,j-1}^{n})\right] \\ & - \frac{i\Delta t}{2}v_{ij}(u_{ij}^{n+1} + u_{ij}^{n}). \end{aligned}$$

Introducing $r = \frac{i\Delta t}{2h^2}$ and collecting terms with u^{n+1} on the left and terms with u^n on the right yields our final discretization:

$$\begin{aligned} & u_{ij}^{n+1} - r(u_{i+1,j}^{n+1} - 2u_{ij}^{n+1} + u_{i-1,j}^{n+1}) \\ & - r(u_{i,j+1}^{n+1} - 2u_{ij}^{n+1} + u_{i,j-1}^{n+1}) + \frac{i\Delta t}{2}v_{ij}u_{ij}^{n+1} = \\ & u_{ij}^{n} + r(u_{i+1,j}^{n} - 2u_{ij}^{n} + u_{i-1,j}^{n}) \\ & + r(u_{i,j+1}^{n} - 2u_{ij}^{n} + u_{i,j-1}^{n}) - \frac{i\Delta t}{2}v_{ij}u_{ij}^{n}. \end{aligned}$$

This scheme maintains second-order accuracy in both space and time, with truncation error $\mathcal{O}(\Delta t^2 + h^2)$. The method preserves unitarity to the same order, ensuring probability conservation during the numerical evolution.

---

[1] Richard P Feynman, Robert B Leighton, and Matthew Sands. *The Feynman Lectures on Physics, Vol. III: Quantum Mechanics*. Addison-Wesley, 1965.

[2] Alain Aspect. Bell's inequality test: more ideal than ever. *Nature*, 398(6724):189–190, 1999.
[3] David J Griffiths and Darrell F Schroeter. *Introduction to Quantum Mechanics*. Cambridge University Press, 2018.
[4] Max Born. Zur quantenmechanik der stoßvorgänge. *Zeitschrift für Physik*, 37(12):863–867, 1926.
[5] Reza Dehghani and Akbar Mohebbi. On the stability of the crank-nicolson scheme for the schrödinger equation. *Journal of Computational Physics*, 231(4):1257–1268, 2012.
[6] John Crank and Phyllis Nicolson. A practical method for numerical evaluation of solutions of partial differential equations of the heat-conduction type. *Mathematical Proceedings of the Cambridge Philosophical Society*, 43(1):50–67, 1947.
[7] Conrad Sanderson and Ryan Curtin. Armadillo: a template-based c++ library for linear algebra. *Journal of Open Source Software*, 1(2):26, 2016.
[8] J. D. Hunter. Matplotlib: A 2d graphics environment. *Computing in Science & Engineering*, 9(3):90–95, 2007.
[9] Michael L Waskom. seaborn: statistical data visualization. *Journal of Open Source Software*, 6(60):3021, 2021.
[10] Anthropic. Claude 3.5 sonnet. https://www.anthropic.com/, 2024. Accessed: March 2024.